ON-LINE CALIBRATION SCHEMES FOR RF-BASED BEAM DIAGNOSTICS

P.-A. Duperrex*, U. Müller, PSI, Villigen, Switzerland

Abstract

RF-based beam diagnostics, such as beam current monitors and beam position monitors (BPMs), rely on precise RF signal measurements. Temperature drifts and differences in the overall measurement chain gain make such measurements very challenging and calibration can drift with time. On-line calibration schemes for BPMs and current monitors have been developed to address these issues. These innovative schemes are based on the use of a pilot signal at a frequency offset from the measurement frequency.

This paper presents the techniques that have been developed to overcome such problems in a proton cyclotron with 2mA current. Results, advantages and disadvantages of such schemes are discussed.

INTRODUCTION

RF-based beam diagnostics rely on precise RF signal measurements. The measurement chain (Fig.1) may comprise one or several sensors, some amplification stages, long cables, some front-end electronics and a processing unit.

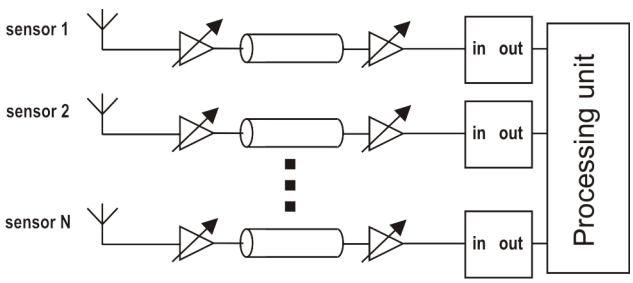

Figure 1: A typical measurement chain with sensors, amplification stages, cabling, signal shaping and processing unit.

To compensate possible different sensor sensitivities, differences between the overall gain of the different lines and electronics temperature drift, calibration procedures are unavoidable. These procedures may require effort and time and need usually to be repeated after repairs. For these reasons, on-line automatized calibration is attractive.

The concept developed for the on-line calibration scheme is to use a test signal (the pilot signal) to calibrate on-line the measurement chain. This has been first applied for a beam current monitor that suffers large gain drifts at high beam intensity. The second application was for calibration of beam position monitors.

ON-LINE CALIBRATION FOR BEAM CURRENT MONITORS

System Description

A beam current monitor, called MHC5, is used to measure the transmission at a 4 cm thick graphite target (the so-called target E) for muon and pion production. Transmission measurements at this point are very important. If a portion of the beam were to bypass the target E, the beam footprint on the next target (the SIN-Q spallation neutron source target) could be reduced. This would lead to an overheating of the SIN-Q target surface. Thus, to avoid such possible damage, the transmission at this point must be carefully monitored.

The MHC5 is placed in vacuum behind the graphite target and is subject to heavy heat load due to the energy deposition of the scattered particles. The resulting mechanical thermal expansion induces a drift of the resonance frequency. Because of the dynamic nature of the calibration drift effect, it was not possible to solve this problem by calibrating the monitor at different beam intensities.

The current monitor (Fig.2) consists of a re-entrant resonator, symmetric around proton beam pipe. The open-end gap in the beam pipe couples some of the wall current into the resonator. This gap acts also as a capacitor and determines the resonance frequency. The resonance frequency is set to 101.26 MHz, the 2nd harmonic of the proton beam bunch frequency. This harmonic is used because of the better signal-to-noise ratio, the RF noise components from the generator being mainly at the odd harmonics. No significant shape dependency of the 2nd harmonic amplitude for relatively short beam pulses is expected [1]. The oscillating magnetic field in the resonator is measured using a magnetic pick-up loop, the signal being proportional to the beam current. Advantages of such resonator are that its construction is simple and it is rugged with respect to radiation. Disadvantages are that it is sensitive to temperature and it is not an absolute measurement; the signal has to be calibrated.

The monitor is made of aluminium (Anticorodal 110), with a 10µm coating layer of silver to improve the electrical conductivity. The inner diameter is 225mm, the outer diameter 420mm, its height 224mm. The capacitor gap is 4mm and small movable plates are used for the fine tuning of the resonance. It has an active water cooling system (maximum water speed: 2m/s).

The monitor itself is in vacuum and the external surfaces were chemically blackened to increase the emissivity for additional cooling.

ISBN 978-3-95450-118-2

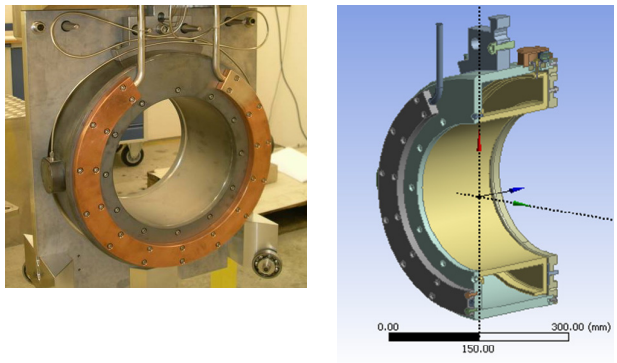

Figure 2: Current monitor ready for installation with the water cooling circuitry at the beam entry side (left). The cavity structure is shown in a half-cut drawing (right).

Resonance Condition and Drift Effects

The monitor can be modelled as a coaxial transmission line with a capacitor shunt. The resonance condition [2] can be expressed as:

$$\tan\left(\frac{2\pi L}{\lambda_m}\right) = \frac{\lambda_m}{2\pi c C_{shunt} Z_o}$$

where L is the resonator length, λ_m the resonant wavelength, Z_o the characteristic impedance of the transmission line and C_{shunt} the shunt capacitor.

For the MHC5, the predicted heat load due to the shower particles is about 230W for a 2mA beam [3]. The monitor would easily reach 200° C without water cooling. With water cooling, the system temperature may vary between 30 to 70 °C.

Any temperature variation affects the resonator geometry, shifts the resonance frequency and modifies the gain at the RF frequency. Bench tests were performed by varying the resonator temperature. Gain drifts smaller than 0.3dB were measured for the expected temperature variations during beam operation, as shown in Fig.3.

However, the observed gain drifts during operation are larger than those measured on the test bench. These larger drifts are induced by the non-uniform temperature distribution, deforming the resonator, shifting the resonance frequency and modifying the gain [3]. It was thus necessary to implement a drift compensation method that could account for these dynamic changes during beam operation.

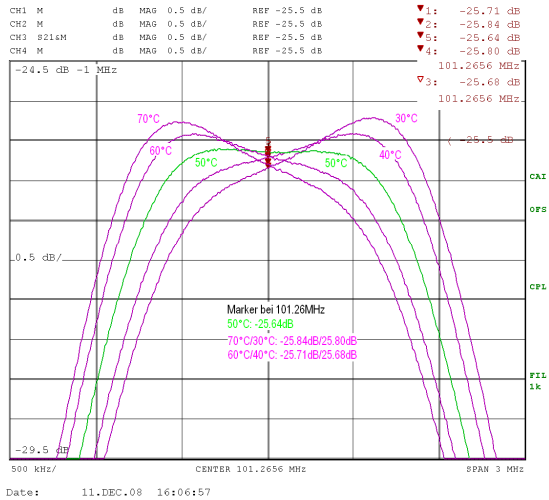

Figure 3: Transfer function of the MHC5 measured at different temperatures. The gain variation at 101.26MHz is smaller than 0.3 dB in laboratory conditions.

Compensation Principle

The principle of this new scheme is to use two pilot signals whose frequency is close enough to the RF 2nd harmonic (101.26MHz) to get an estimate of the resonator gain at the RF 2nd harmonic.

The two pilot signals are feed into the resonator and measured using a second magnetic pick-up loop identical to the one used for the current measurement. The comparison of the pilot signal amplitude at the receiver side with the one at the emitter side is a measure of the resonator gain at the pilot frequency. The results obtained at the two different pilot frequencies can then be averaged and give that way an estimate of the resonator gain at the RF frequency.

The frequency difference between the pilot signals and the beam signal has to be large enough to avoid interference with the standard current monitor electronics but small enough so that the average of the two pilot signals can provide a good estimate of the gain.

Electronics and Signal Processing

The initial electronics schematic is shown in Fig.4. A 52 kHz baseband signal is mixed with the second RF harmonic to generate two pilot signals 52kHz off the 101.26MHz frequency. The resulting signal is fed into the current monitor resonator. These pilot signals are then measured using as sensor a pick-up coil identical to the one used for the current measurements.

To separate the amplitude of both pilot signals, a double image rejection mixer (Fig.5) has been used. It is an I/Q demodulator followed by a couple of 90 degree phase shifters before a recombination of the demodulated signals.

ISBN 978-3-95450-118-2

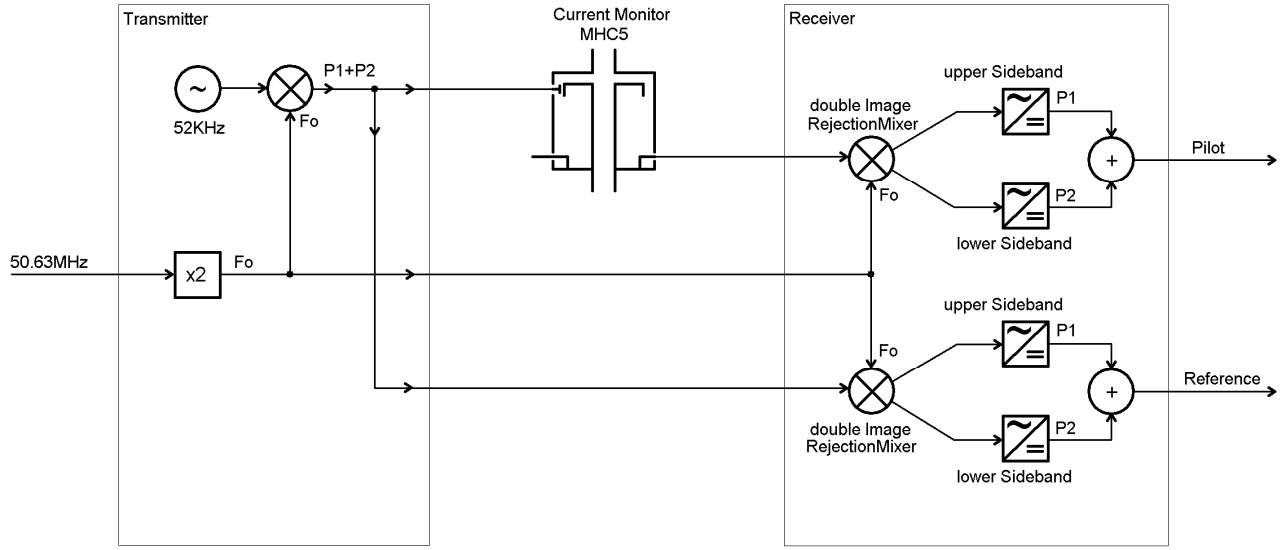

Figure 4: Schematic of signal measurements for the on-line drift compensation. A 52 kHz baseband signal is mixed with the second RF harmonic and feed into the current monitor resonator. The signals are then measured using double image rejection mixers. The ratio Pilot/Reference provides an estimate of the resonator gain.

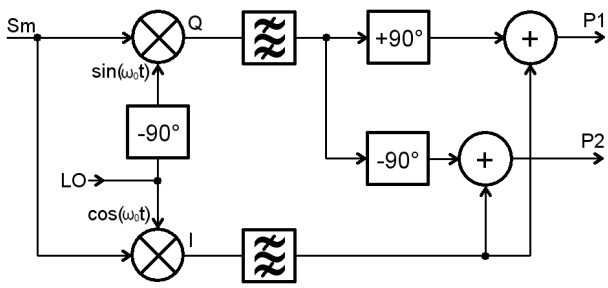

Figure 5: Details of the double image rejection scheme. The Q demodulated component is phase shifted and the resulting signals are recombined with the in-phase signal.

The results can be derived analytically as follows. The measured pick-up signal S_m contains the two pilot signals as well as the beam signal:

$$S_m = P_{10}.\cos(\omega_1.t+\phi_1)+P_{20}.\cos(\omega_2.t+\phi_2)+S_{beam}.\cos(\omega_0.t)$$

where ω_o the angular frequency of the RF 2nd harmonic, $\omega_1=\omega_o-\Delta\omega$ and $\omega_2=\omega_o+\Delta\omega$ the angular frequency of the pilot signals, with $\Delta\omega/2\pi$=52 kHz, P_{10} (resp. P_{20}) the amplitude of the first (resp. second) pilot signal and S_{beam} the amplitude of the beam signal.

After mixing down the signals with the image rejection, a band-pass filter centered at the original pilot frequency eliminates the undesired high frequency components and as well as the beam signal contribution (DC component).

The resulting base-band in-phase (I) and quadrature phase (Q) signals are then:

$$S_I(t)=\frac{1}{2}P_{10}.\cos(\Delta\omega.t-\phi_1)+\frac{1}{2}P_{20}.\cos(\Delta\omega.t+\phi_2)$$

$$S_Q(t)=\frac{1}{2}P_{10}.\sin(\Delta\omega.t-\phi_1)-\frac{1}{2}P_{20}.\sin(\Delta\omega.t+\phi_2)$$

By introducing 90degree phase shifts on the Q output:

$$S_{Q+90\deg}(t)=\frac{1}{2}P_{10}.\cos(\Delta\omega.t-\phi_1)-\frac{1}{2}P_{20}.\cos(\Delta\omega.t+\phi_2)$$

$$S_{Q-90\deg}(t)=-\frac{1}{2}P_{10}.\cos(\Delta\omega.t-\phi_1)+\frac{1}{2}P_{20}.\cos(\Delta\omega.t+\phi_2)$$

The two pilot signals can then be extracted:

$$S_I(t)+S_{Q+90\deg}(t)=P_{10}.\cos(\Delta\omega.t-\phi_1)$$

$$S_I(t)+S_{Q-90\deg}(t)=P_{20}.\cos(\Delta\omega.t+\phi_2)$$

This way, the pilot signals are separated and their amplitude independently measured. An average is then performed to estimate the level of a pilot signal at 101.26MHz.

After digitization of the averaged pilot and reference signals the Reference/Pilot ratio is then calculated and used as additional scaling factor for the MHC5 current signal:

$$MHC5_{calibrated}=K.\frac{S_{Reference}}{S_{Pilot}}.MHC5_{raw}$$

K being a constant calibration factor that is determined once for all at the beginning of the measurements. Compared to the first version developed two years ago [4], the new version shown in Fig.4 has in addition an I/Q demodulation for the reference signal to improve the long time stability of the measurements.

Results

The calibration factor calculated with the pilot drift compensation scheme was compared during 3 days with the one that can be deduced using the MHC6 current monitor (Fig.6). Such comparison is sometime possible because the MHC6 is located further down the beam line after a steering magnet, which directs the beam to either a beam dump or the spallation neutron source. Depending of the beam operation the MHC6 current monitor may see the same beam current. The MHC6 is not subject to such

ISBN 978-3-95450-118-2

heat load and delivers stable measurements. Thus, depending of the beam operation conditions, the MHC5 scale factor may also be deduced from the MHC6. In the example shown in figure 6, the MHC5 cooling system was switched off after 2.5days of operation. The MHC5 temperature rose from 40 to 90°C and the calibration factor changed by 30%. Even during this critical phase, the calibration measured with the pilot scheme perfectly matched the calibration deduced from the MHC6.

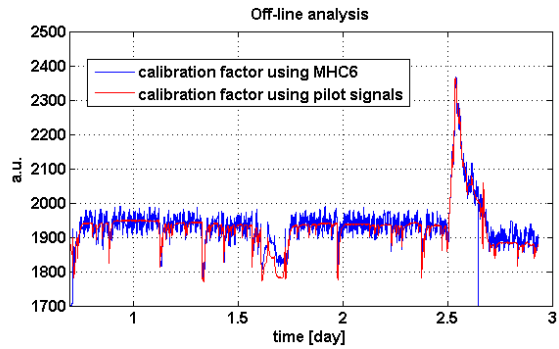

Figure 6: Off-line calibration. Even for a 30% variation, the calibration factor deduced from the pilot signals (red line) matches the one using MHC6, a second current monitor (blue line) further down the beam line.

ON-LINE CALIBRATION FOR BEAM POSITION MONITOR SYSTEMS

BPM System Description

Beam position monitors (BPM) rely on the measurements of inductive or capacitive pickup signals located on either side of the beam. The quality of the measurements depends on the correct calibration of the measurement chain over the whole dynamic range, a challenge when using for instance voltage controlled amplifiers.

The position is calculated by applying the difference over the sum method:

$$\Delta x = K.\frac{S^+ - S^-}{S^+ + S^-}$$

where S^+ and S^- are the opposite magnetic pickups signal levels at the second RF harmonics (101.26 MHz) and K a calibration parameter.

The electronics is based on digital receiver techniques. After a first amplification stage (HFFE) to maximize the signal-to-noise ratio (SNR) and about 75 to 100 m cables, the pickup signals are digitized using fast 14 bit AD6644 ADCs. The ISL5216 digital down converter (DDC) translates the signals into the baseband. Compared to a standard solution (upper plot, Fig.7), the HFFE adds a pilot signal at a frequency very close to the beam signal frequency (lower plot, Fig.7). In this way, the pilot signals provide a direct measurement of the whole measurement chain, except the sensor itself. The calculation of the beam position may be reformulated as followed:

$$\Delta x = K.\frac{S_n^+ - S_n^-}{S_n^+ + S_n^-}$$

Where S_n^+ and S_n^- are the signals from the sensor + or – respectively normalized by the corresponding pilot signal:

$$S_n^+ = \frac{S_{beam}^+}{S_{pilot}^+} \text{ and } S_n^- = \frac{S_{beam}^-}{S_{pilot}^-}$$

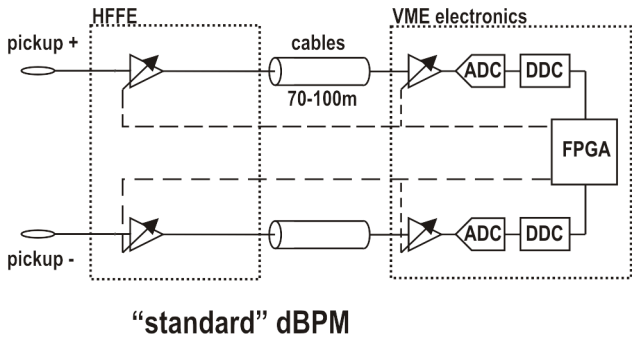

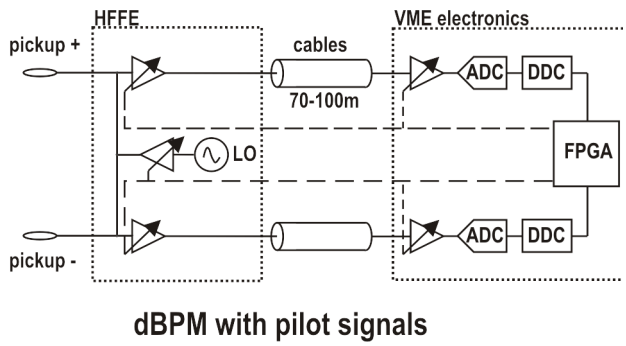

Figure 7: Measurement chain for a standard solution (upper plot) and with an on-line calibration scheme using a pilot signal (lower plot).

Signal Normalization as Interference Cancelling

It was expected that the normalization scheme would degrade the signal-to-noise ratio (SNR). For that reason, the noise level of the raw and normalized signals was compared (Fig.8).

It appeared that the relative standard deviation of the normalised signal (1%) is smaller by a factor 4: the normalization actually improves the signal-to-noise ratio (SNR).

The reason of the surprising SNR improvement has been investigated by computing the coherence spectra for different signal combinations. The coherence function [5] is defined as:

$$C_{xy}(f) = \frac{|P_{xy}(f)|^2}{P_{xx}(f) \cdot P_{yy}(f)}$$

ISBN 978-3-95450-118-2

with $P_{xx}(f)$ $P_{yy}(f)$ the power spectral density of x and y and $P_{xy}(f)$ the cross power spectral density. The function $C_{xy}(f)$ indicates how well the signal frequency components are correlated.

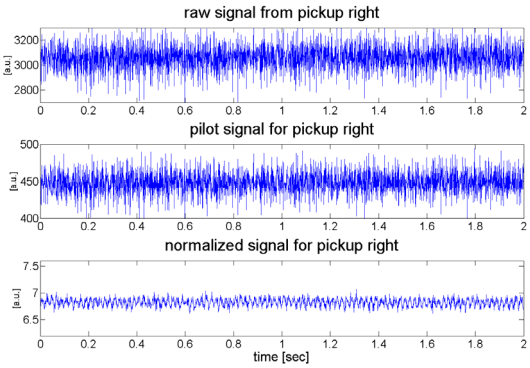

Figure 8: Time evolution of the raw beam signal, pilot signal and normalized signal. The standard deviation for the normalized signal (1%) is smaller by about a factor 4.

For the results presented here, the coherence has been computed with MATLAB applying the Welch method with 50% overlap. The effective sampling frequency was 1kHz. The MXS3 BPM has been used for these measurements at a beam current of 1.97 mA.

The beam and pilot signals are well correlated for the horizontal direction. Fig.9 shows an example for the coherence spectrum between beam and pilot signal of the right pickup coil. Similar results have been obtained in the vertical direction. However no correlation has been observed between horizontal and vertical signals.

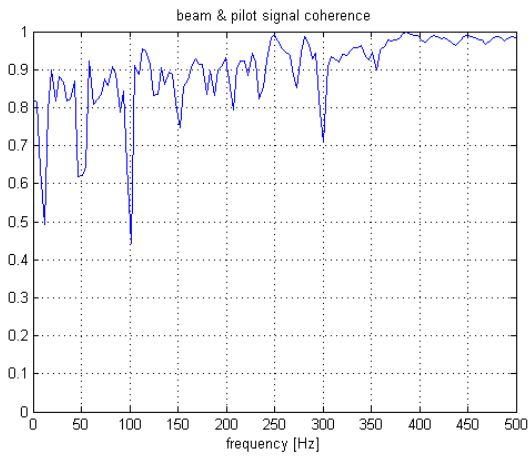

Figure 9: coherence spectrum of the beam & pilot signal for the right pickup coil showing their strong correlation.

This suggests that the observed beam or pilot signal noise is of instrumental origin. It is interesting to notice that the normalized signals exhibit some correlation only for the 50Hz harmonics (Fig.10). The coherence results explain why the noise is reduced for the normalized signals. Because the noise is similar for the raw beam and pilots signals, the signal normalization acts as a filter. The noise is almost cancelled.

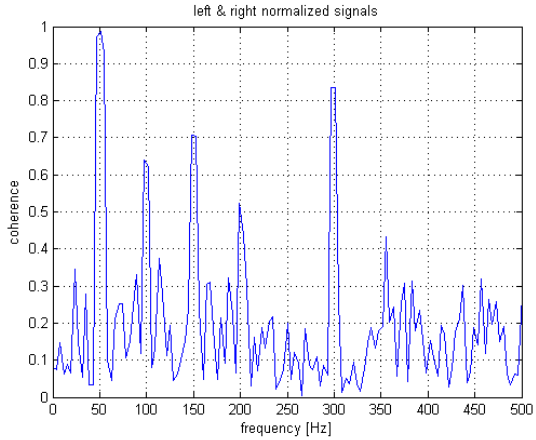

Figure 10: Coherence: no correlation between left and right normalized signals, except the 50Hz harmonics.

SUMMARY AND CONCLUSION

Two examples of an on-line calibration scheme have been presented. It has been shown that it offers large accuracy improvements for sensors such as resonators affected by gain drifts due to temperature effects and removes the need for separate calibration procedures. For BPMs it has been shown that the beam and pilot signals are well correlated, so the scheme improves the signal-to-noise ratio (SNR).

The drawback of such schemes is a more complex measurement system. In the future, a higher performance scheme may be developed using adaptive filtering or interference cancelling [6] and benefiting from the latest FPGA und electronic technology.

REFERENCES

[1] R. Reimann, M. Rüede, “Strommonitor für die Messung eines gepulsten Ionenstrahls”, Nucl. Instr. Meth. 129 (1975) 53.

[2] P.-A. Duperrex, P. Baumann, S. Joray, D. Kiselev, Y. Lee, U. Müller, „Design and operation of a current monitor under heavy heat load” DIPAC’2009, May 2009, TUPD20, p.336 (2009).

[3] Y. Lee "Simulation based Analysis of the anomalous RF drifts of a Current Monitor at the PSI Proton Accelerator Facilities", IPAC2010, May 2010, MOPEC072.

[4] P.-A. Duperrex, M. Gandel, D. Kiselev, Y. Lee, U. Müller, "Current and Transmission measurement challenges for high intensity beams”, HB2010, Sept.2010, WEO2A04.

[5] J. S. Bendat, A. G. Piersol, “Engineering Applications of Correlation and Spectral Analysis”, John Wiley & Sons, p.72.

[6] J.R. Widrow et al, “Adaptive noise cancelling: Principles and applications”, Proceedings of the IEEE, Vol.63, issue 12, 1692-1716.

ISBN 978-3-95450-118-2